Neuron, Volume *111*

Supplemental information

Genetically encoded sensors for measuring histamine release both *in vitro* and *in vivo*

Hui Dong, Mengyao Li, Yuqi Yan, Tongrui Qian, Yunzhi Lin, Xiaoyuan Ma, Henry F. Vischer, Can Liu, Guochuan Li, Huan Wang, Rob Leurs, and Yulong Li

Figure S1

A

HRHs	Reported EC_{50} (nM)	Refs
hH_1R	~2000 - 80000	S1, S2, and S3
hH_2R	~300 - 50000	S4 and S5
hH_3R	~6 - 25	S6, S7, and S8
hH_4R	~9 - 25	S5 and S8

B

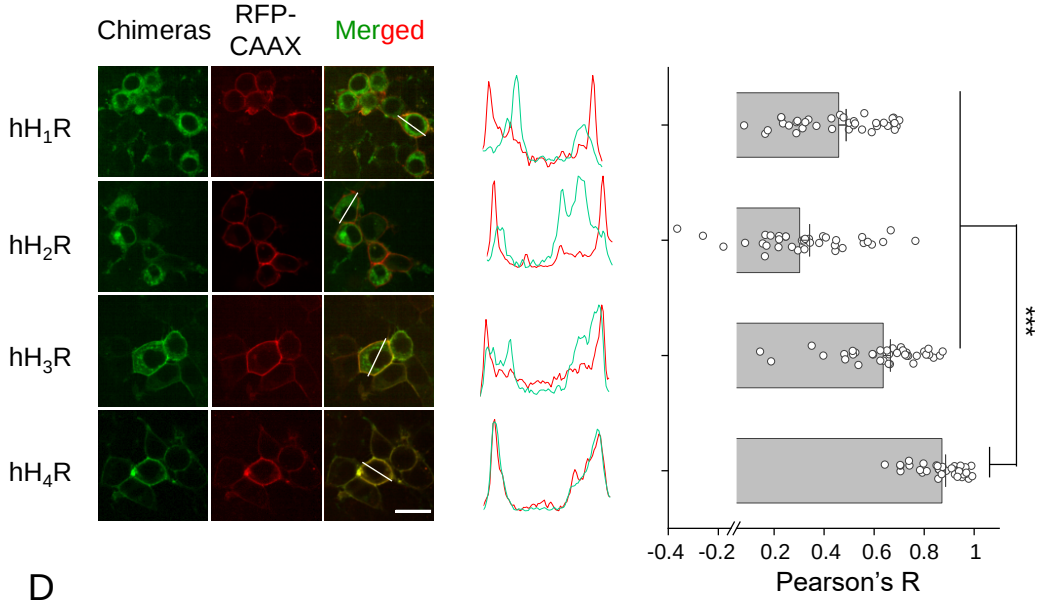

C

Sensors	EC_{50} to HA (nM)
HA1h	~17
HA1m	~380
HA1mut	n.d.

D

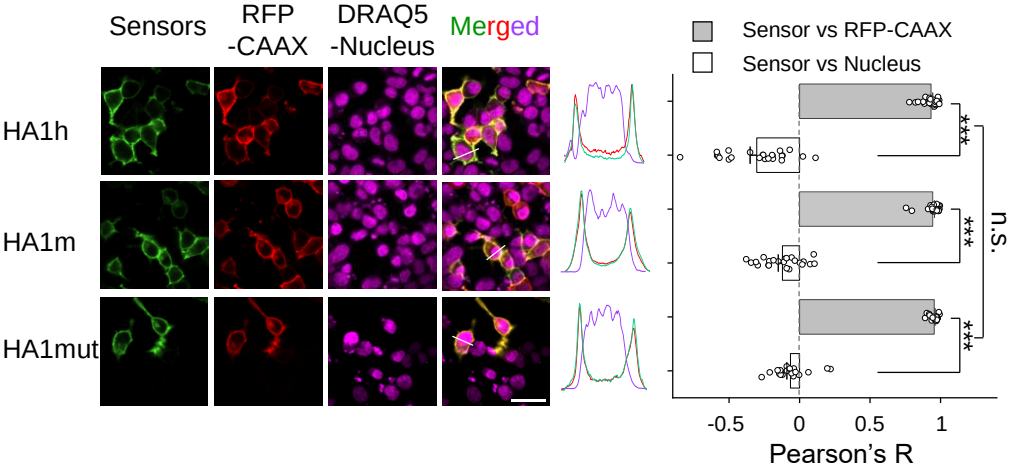

Figure S1. Plasma membrane trafficking profile of the initial prototypes and the finalized sensors in cultured HEK293T cells, related to Figure 1.

(A) Summary of the reported EC_{50} values for the indicated human HA receptors (source: https://www.guidetopharmacology.org/GRAC/LigandActivityRangeVisForward?ligandId=1204).

(B) Analysis of fluorescence and membrane trafficking of all four human HA receptors containing cpEGFP expressed in HEK293T cells; membrane-targeted RFP (RFP-CAAX) was co-expressed to label the plasma membrane. Left, fluorescence images of HEK293T cells expressing the indicated HA receptor-based chimeras (green) and RFP (red). Middle, normalized line-scanning plots of the fluorescence signals measured in both the green and red channels. Right, summary of Pearson's co-localization ratio measured between the indicated HA receptor-based chimeras and RFP-CAAX; *** P <0.001 versus hH_4R. Scale bar, 20 μm.

(C) Summary of the EC_{50} values for the indicated HA sensors to HA in cultured HEK293T cells. n.d., not determined

(D) Plasma membrane trafficking profile of the final design sensors in cultured HEK293T cells. Left, fluorescence images of HEK293T cells expressing the indicated HA sensor (green), RFP-CAAX (red), and nuclear dye DRAQ5 (purple). Middle, normalized line-scanning plots of the fluorescence signals measured in both the green, red, and purple channels. Right, summary of Pearson's co-localization ratio measured between the indicated HA sensor and RFP-CAAX or nuclear dye. Scale bar, 50 μm. n = 23, 23, and 24 cells from 3 wells for HA1h, HA1m, and HA1mut, respectively.

Figure S2

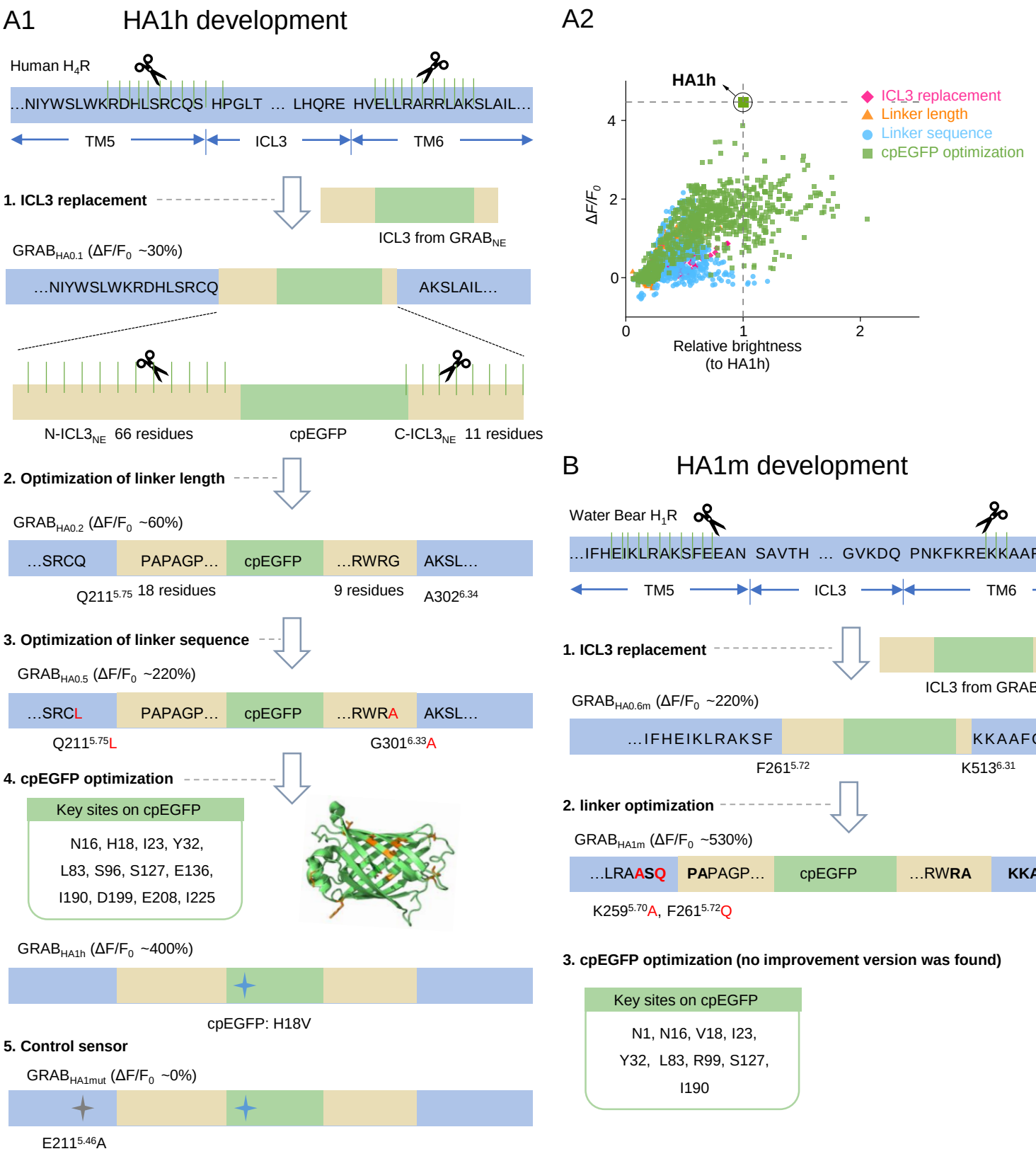

Figure S2. Strategy for optimizing and screening the GRAB$_{HA}$ sensors, related to Figure 1.
(A1) A flowchart showing the development process of the GRAB$_{HA1h}$ and GRAB$_{HA1mut}$ sensors. Responses to 10 μM HA of candidate sensors were shown alongside each step.
(A2) Optimization of candidate HA sensors based on the human H_1R.
(B) A flowchart showing the development process of the GRAB$_{HA1m}$ sensor. Responses to 100 μM HA of candidate sensors were shown alongside each step.

Figure S3

A

GRAB$_{HA1h}$

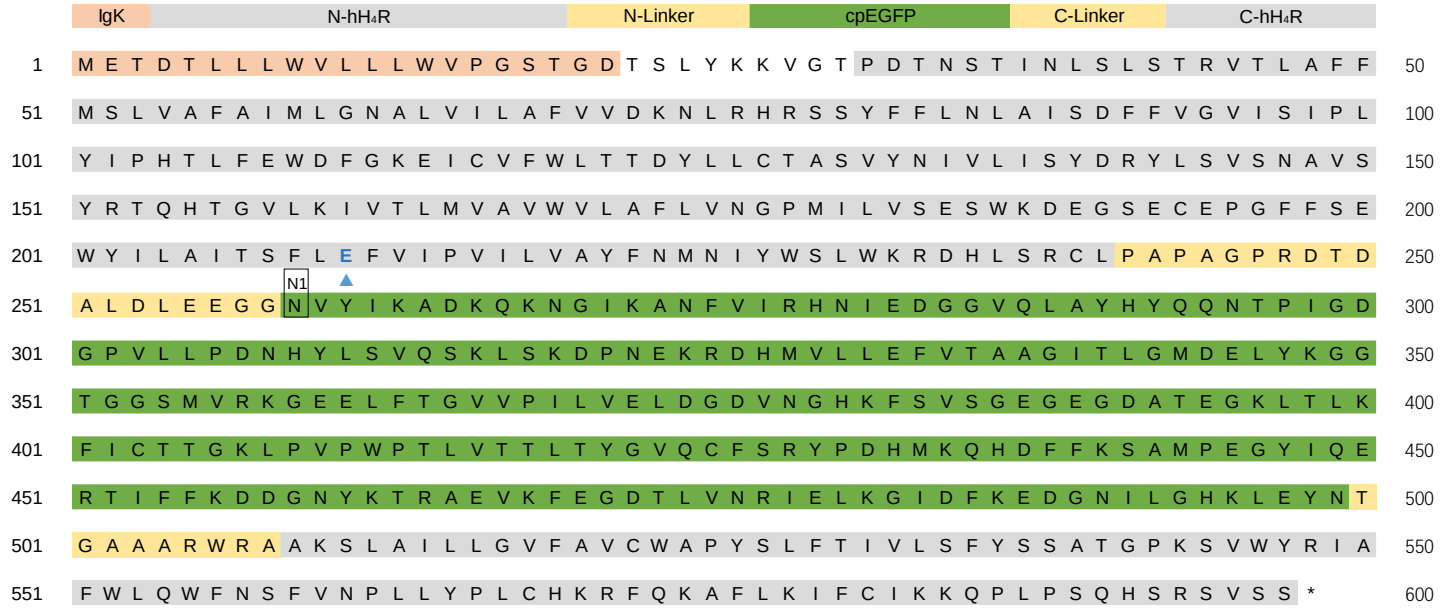

HA1mut site:

E211$^{5.46}$A

B

GRAB$_{HA1m}$

C

Sensor/Fluorescent protein		N1	N16	H18	I23	Y32	L83	S96	R99	S127	E136	I190	D199	E208	I225
GPCR based	GRAB$_{HA1h}$	N	N	V	I	Y	L	S	R	S	E	I	D	E	I
	GRAB$_{HA1m}$	N	N	V	I	Y	L	S	R	S	E	I	D	E	I
	GRAB$_{NE1m}$	N	N	H	I	Y	L	S	R	S	E	I	D	E	I
	GRAB$_{DA2m}$	T	N	H	I	Y	L	S	S	S	Y	I	D	E	I
	GRAB$_{ACh3.0}$	N	N	H	I	Y	N	S	R	T	I	I	G	I	I
	dLight1.1	N	N	K	I	Y	L	S	S	S	Y	I	D	E	I
Other protein based	GCaMP8m	N	N	H	I	Y	L	S	S	S	Y	I	D	E	I
	iGluSnFR3	T	N	K	V	D	L	S	S	R	N	V	D	E	I
	ASAP3	N	N	T	V	D	H	S	S	R	I	V	D	V	I
Fluorescent protein	sfGFP	N	N	K	V	D	H	-	S	R	N	V	D	E	I
	mClover3	Y	N	K	V	D	H	-	S	R	N	V	D	E	I

Figure S3. The amino acid sequences of the GRAB$_{HA}$ sensors, related to Figure 1.

(A, B) The amino acid sequences of the $GRAB_{HA1h}$ (A) and $GRAB_{HA1m}$ (B) sensors are shown, with the indicated domains shown above. Also shown is the location of the E211A mutation (blue arrowhead) in $GRAB_{HA1h}$ to generate the $GRAB_{HA1mut}$ sensor. The N1 of cpEGFP is indicated by the black box.
(C) The summary of amino acids in cpEGFP in different genetically encoded sensors and fluorescent protein, including GPCR-based sensors and other protein backbone-based sensors. Amino acids shaded in green and gray indicate identical and different residues, respectively.

Figure S4

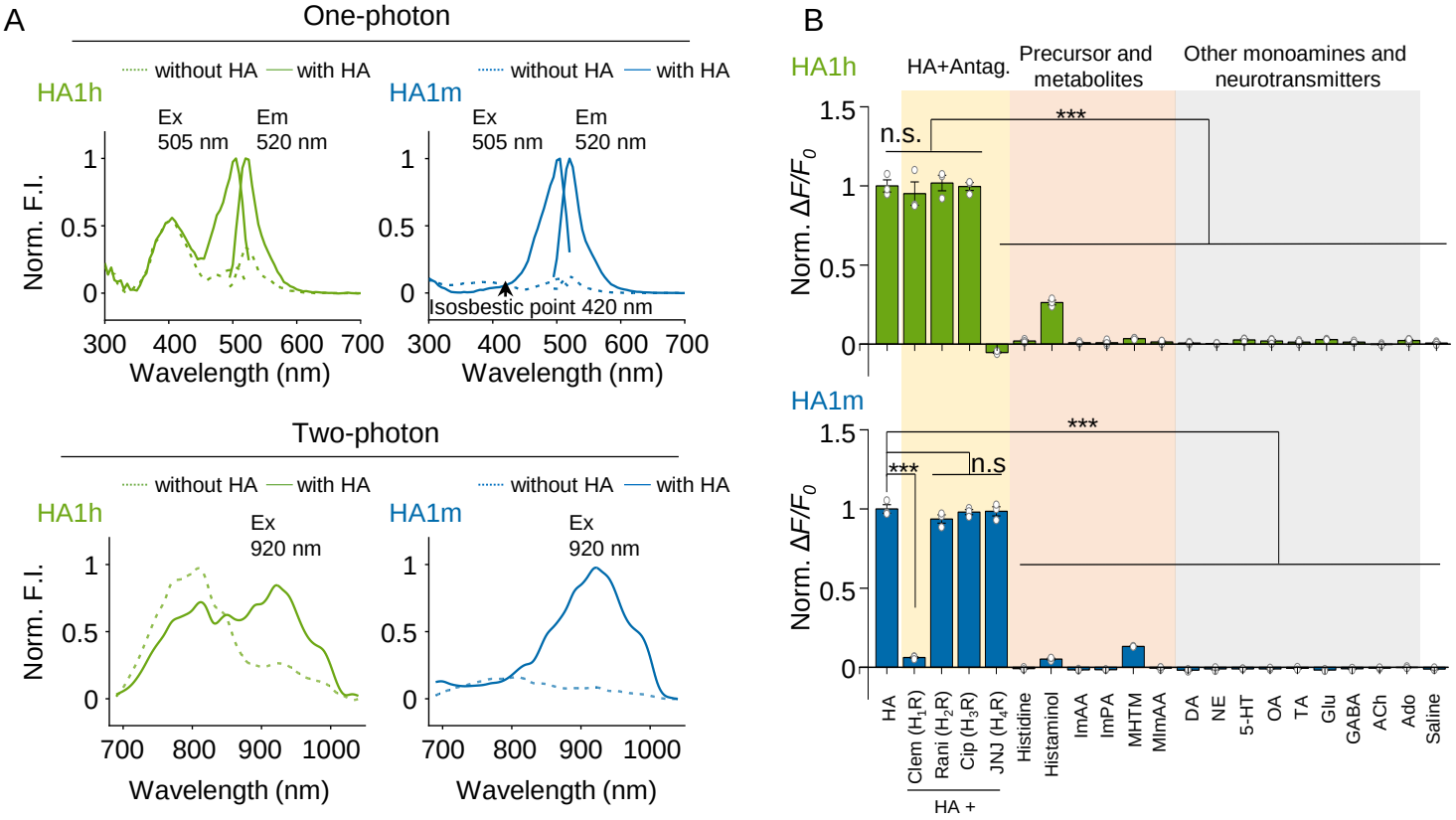

Figure S4. Characterization of the wavelength spectra and specificity of HA sensors expressed in cultured HEK293T cells, related to Figure 2.

(A) One-photon excitation (Ex) and emission (Em) spectra (top panel) and two-photon excitation spectra (bottom panel) of HA1h and HA1m measured in the absence and presence of HA.

(B) Summary of the normalized change in fluorescence measured for HA1h (top panel) and HA1m (bottom panel) expressed in cultured HEK293T cells in response to the indicated compounds (applied at 5 μM each); see Figure 2 for abbreviations. $n = 3$ wells for different groups. Paired two-tailed Student's t-tests were performed. *** $P < 0.001$; n.s., not significant.

Figure S5

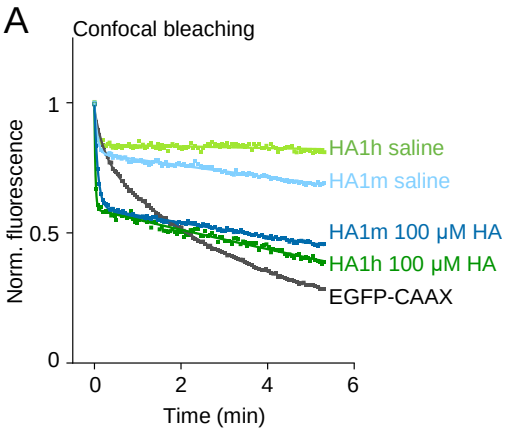

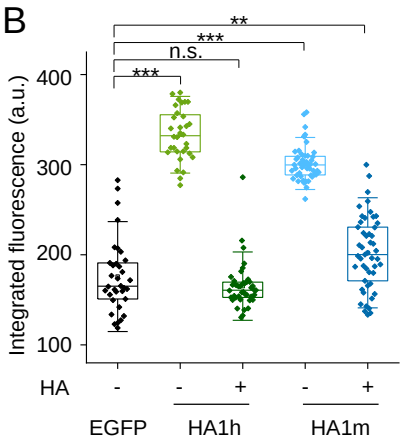

C

	Tau fast (s)	% fast	Tau slow (s)	% slow
EGFP-CAAX	11	29.7	173	70.3
HA1h saline	5.2	51.2	192	48.8
HA1h HA	1.2	54.4	451	45.6
HA1m saline	4.5	49.3	392	50.7
HA1m HA	1.4	52.4	1129	47.6

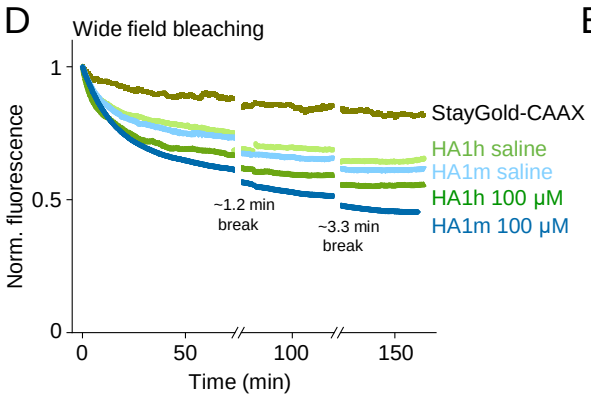

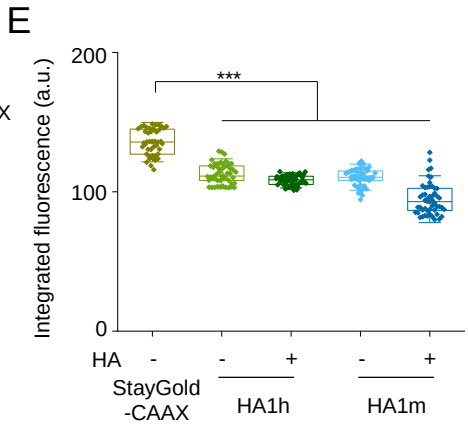

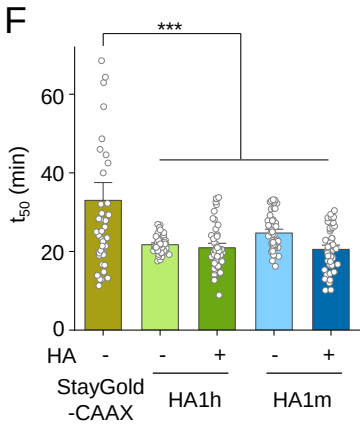

Figure S5. Photostability of GRAB$_{HA}$ sensors, related to Figure 2.
(A-C) Photostability measurement under confocal bleaching condition. (A), Normalized fluorescence of EGFP-CAAX, or HA1h and HA1m (in the absence and presence of 100 μM HA) in the cultured HEK293T cells during confocal laser bleaching. (B), Integrated fluorescence of EGFP-CAAX, or HA1h and HA1m (in the absence and presence of 100 μM HA) shown in (A). *n* = 4 cultures. Boxes show the first and third quartiles as well as the median. (C), Fast and slow time constants and component amplitudes of EGFP or corresponding sensor traces fit by double exponentials. Two-tailed Student's t-tests were performed. ** $P < 0.01$, *** $P < 0.001$; n.s., not significant.
(D-F) Photostability measurement under wide field bleaching condition. (D), Normalized fluorescence of StayGold-CAAX, or HA1h and HA1m (in the absence and presence of 100 μM HA) in the cultured HEK293T cells during wide field LED bleaching. Breaks (in D) are due to the time limitation of the illumination system. (E), Integrated fluorescence of StayGold-CAAX, or HA1h and HA1m (in the absence and presence of 100 μM HA) shown in (D). (F), t_{50} of StayGold or corresponding sensor traces. *n* = 3 cultures. Two-tailed Student's t-tests were performed. *** $P < 0.001$.

Figure S6

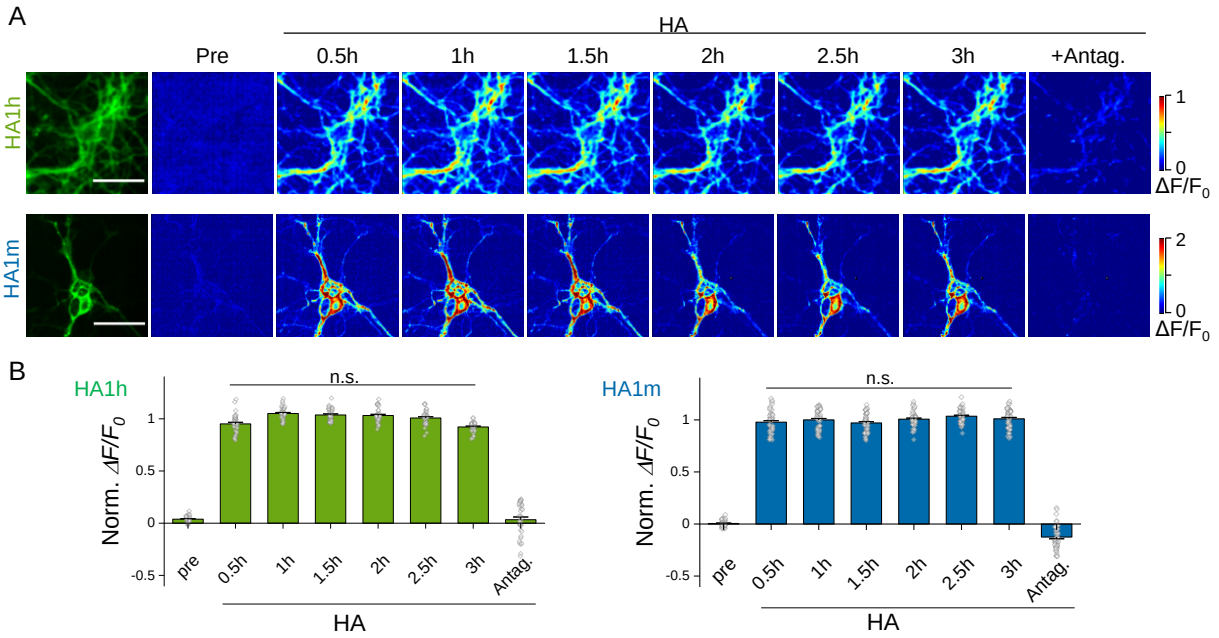

Figure S6. 3-h recording of HA1h and HA1m expressed in cultured cortical neurons, related to Figure 2.
Shown are fluorescence images (A) and summary data (B) of the indicated HA sensors expressed in cultured neurons before (Pre) and during a 3-h application of HA at saturating concentration, followed by application of the corresponding antagonist. *n* = 3 wells for each group.

Figure S7

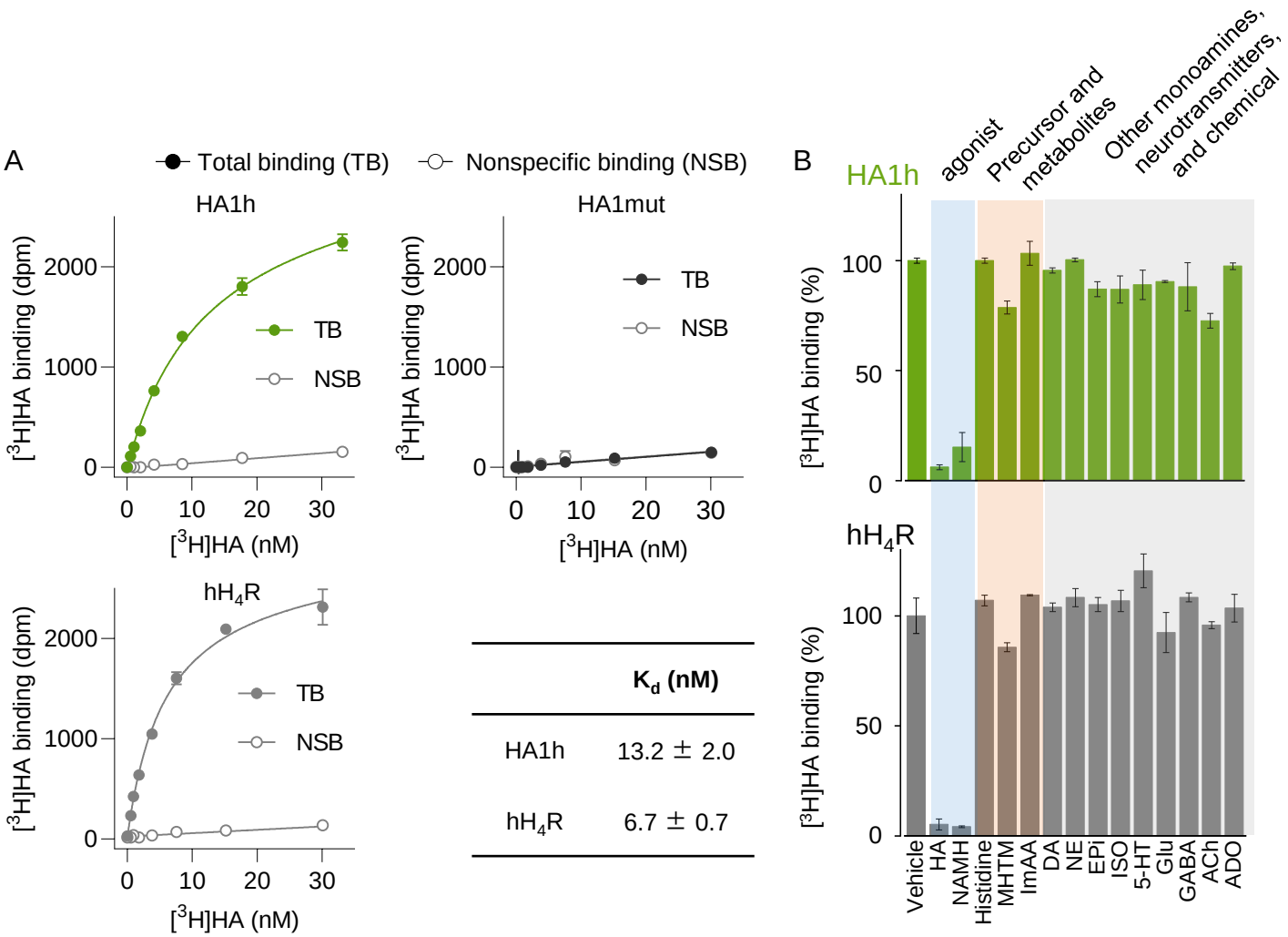

	K_d (nM)
HA1h	13.2 ± 2.0
hH_4R	6.7 ± 0.7

Figure S7. [^{3}H]HA radioligand binding assay for HA1h sensor, related to Figures 1 and 2.
(A) Binding affinity measurement. Specific binding of increasing concentrations [^{3}H]HA to HEK293T cell homogenates expressing HA1h, HA1mut, or hH_4R. TB: total binding, NSB: nonspecific binding.
(B) [^{3}H]HA radioligand competition binding assay for measurement of [^{3}H]HA (8.5 nM) binding to test whether HA, H_4R agonist, HA precursor, HA metabolites, and other monoamines, neurotransmitters, and chemicals (all compounds were applied at 30 μM) bind to HA1h sensor (top panel) and WT hH_4R (bottom panel).

Figure S8

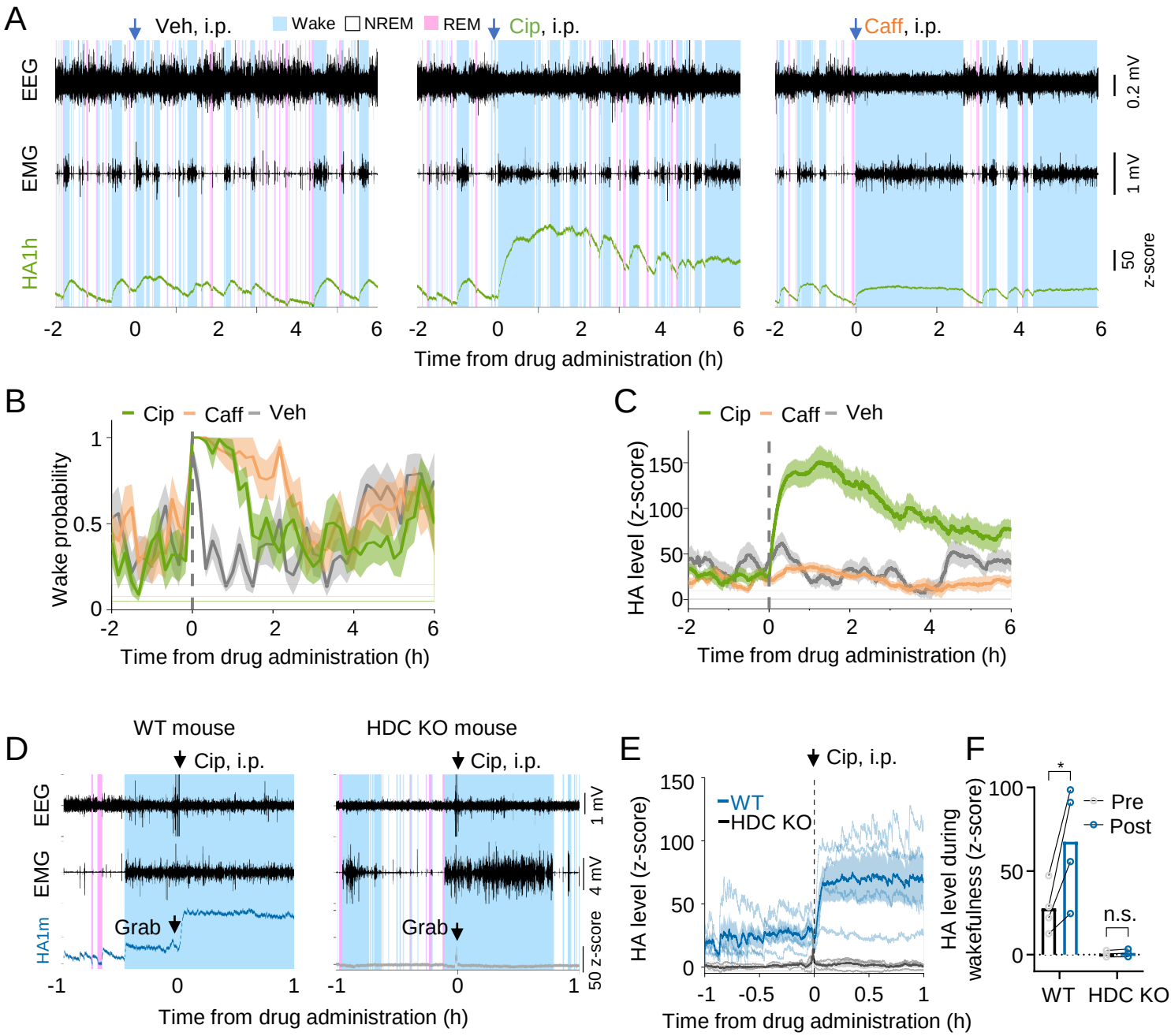

Figure S8. Wake-promoting agent, H_3R antagonist, enhanced HA level in the PFC of mice, related to Figures 4 and 5.

(A) Typical traces of EEG, EMG and HA1h signals after administration of wake-promoting agents, H3R antagonist, ciproxifan at 3 mg/kg, or caffeine at 15 mg/kg, or vehicle in WT mice, extend shown time in Figure 5I.

(B) Time courses of wake probability before and after administration of ciproxifan, caffeine and vehicle, extend shown time in Figure 5J.

(C) Time courses of HA1h signals before and after administration of ciproxifan, caffeine and vehicle, extend shown time in Figure 5K.

(D) Typical traces of EEG, EMG and HA1m signals after administration of H3R antagonist, ciproxifan at 3 mg/kg in WT mouse (left panel) and HDC KO mouse (right panel).

(E) Time courses of HA1m signals before and after administration of ciproxifan in WT mouse and HDC KO mouse.

(F) Ground data of HA1m signals before and after administration of ciproxifan in WT mouse and HDC KO mouse. Two-way ANOVA between genotype and time; F(time) = 9.6457, P = 0.0267, pre-post comparisons followed by Sidak's test WT pre vs post P = 0.0107, HDC KO pre vs post P = 0.9989;

Figure S9

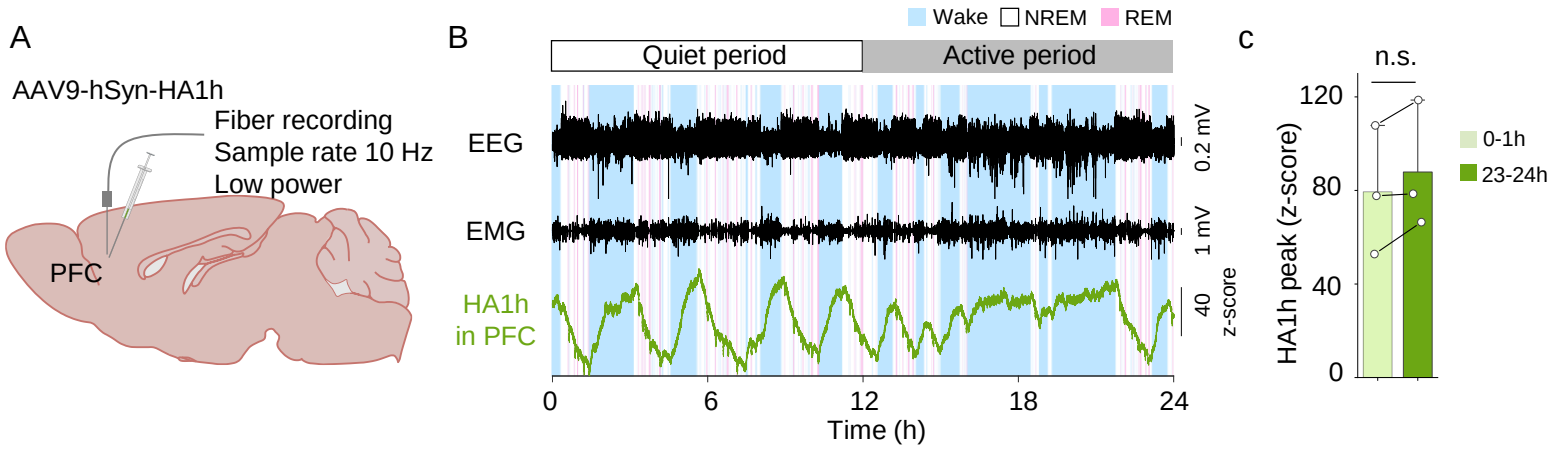

Figure S9. HA1h can be used to measure HA dynamics over one day *in vivo*, related to Figure 5.
(A) Schematic diagram depicting Simultaneous recording of HA1h in the PFC and POA during sleep–wake cycles.
(B) Typical traces of EEG, EMG and HA1h signals over 24h. The brain states are color-coded.
(C) Summary data of first and last hour averaged HA1h peak signals. Paired two-tailed Student's t-tests were performed. $t = 2.184$, $P = 0.161$; n.s., not significant.

Figure S10

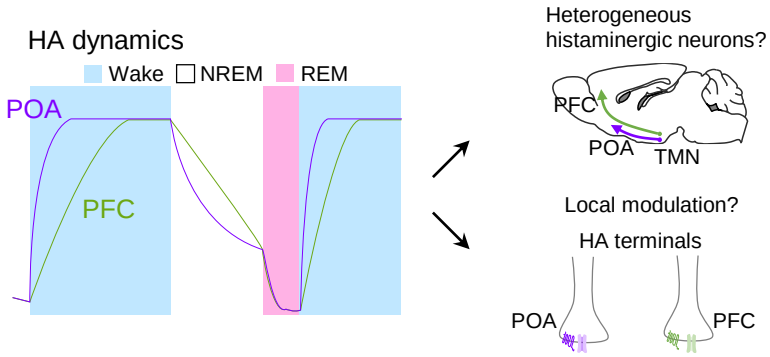

Figure S10. Model depicting two possible explanations for the difference in HA release kinetics between the POA and PFC, related to Figure 6.

SUPPLEMENTAL REFERENCES

1. Seifert, R., Wenzel-Seifert, K., Burckstummer, T., Pertz, H.H., Schunack, W., Dove, S., Buschauer, A., and Elz, S. (2003). Multiple differences in agonist and antagonist pharmacology between human and guinea pig histamine H1-receptor. J Pharmacol Exp Ther *305*, 1104-1115. 10.1124/jpet.103.049619.
2. Jongejan, A., Bruysters, M., Ballesteros, J.A., Haaksma, E., Bakker, R.A., Pardo, L., and Leurs, R. (2005). Linking agonist binding to histamine H1 receptor activation. Nat Chem Biol *1*, 98-103. 10.1038/nchembio714.
3. Xie, S.-X., Ghorai, P., Ye, Q.-Z., Buschauer, A., and Seifert, R. (2006). Probing Ligand-Specific Histamine H1- and H2-Receptor Conformations withNG-Acylated Imidazolylpropylguanidines. Journal of Pharmacology and Experimental Therapeutics *317*, 139-146. 10.1124/jpet.105.097923.
4. Igel, P., Dove, S., and Buschauer, A. (2010). Histamine H4 receptor agonists. Bioorg Med Chem Lett *20*, 7191-7199. 10.1016/j.bmcl.2010.10.041.
5. Pockes, S., Wifling, D., Keller, M., Buschauer, A., and Elz, S. (2018). Highly Potent, Stable, and Selective Dimeric Hetarylpropylguanidine-Type Histamine H2 Receptor Agonists. ACS Omega *3*, 2865-2882. 10.1021/acsomega.8b00128.
6. Lovenberg, T.W., Pyati, J., Chang, H., Wilson, S.J., and Erlander, M.G. (2000). Cloning of rat histamine H(3) receptor reveals distinct species pharmacological profiles. J Pharmacol Exp Ther *293*, 771-778.
7. CogÉ, F., GuÉNin, S.-P., Audinot, V., Renouard-Try, A., Beauverger, P., Macia, C., Ouvry, C., Nagel, N., Rique, H., Boutin, J.A., and Galizzi, J.-P. (2001). Genomic organization and characterization of splice variants of the human histamine H3 receptor. Biochemical Journal *355*. 10.1042/bj3550279.
8. Deml, K.-F., Beermann, S., Neumann, D., Strasser, A., and Seifert, R. (2009). Interactions of Histamine H1-Receptor Agonists and Antagonists with the Human Histamine H4-Receptor. Molecular Pharmacology *76*, 1019-1030. 10.1124/mol.109.058651.